PCCP

PAPER

View Article Online
View Journal | View Issue

Cite this: *Phys. Chem. Chem. Phys.*, 2016, **18**, 11829

Understanding conductivity in molecular switches: a real space approach in octaphyrins†

T. Woller,[ab] N. Ramos-Berdullas,[c] M. Mandado,[c] M. Alonso,[a] F. de Proft[a] and J. Contreras-García*[bd]

In recent years, expanded porphyrins have emerged as a promising class of π-conjugated molecules that display unique electronic, optical and conformational properties. Several expanded porphyrins can switch between planar and twisted conformations, which have different photophysical properties. Such a change of topology involves a Hückel–Möbius aromaticity switch in a single molecule and it can be induced by solvent, pH and metallation. These features make expanded porphyrins suitable for the development of a novel type of molecular switches for molecular electronic devices. Octaphyrins consisting of eight pyrrole rings, exhibit twisted-Hückel, Möbius and Hückel π-conjugation topologies depending on the oxidation and protonation state, with distinct electronic structures and aromaticity. Our working hypothesis is that a significant change in the conductance of expanded porphyrins will be observed after the topology switching. Despite the potential of Hückel–Möbius systems as conductance switches, the relationship between the conductance and the molecular topology is not yet understood. We have explored the performance of local descriptors of conductivity in simple molecules, as well as the relationship with conductance. Since these indexes provide a qualitative measure of delocalization and conductance in the probe molecules, we have carried out a local analysis of electrical conductance changes as a function of the π-conjugation in two examples. In one of them, the locality of the electronic changes ensures the ability of these indexes to describe the conductance as local. Moreover, it enables to identify which conformational switch would be more efficient from an electronic device perspective. However, we also show that it is not always possible to reduce conductance changes to one bond, and in those molecules where a deep rearrangement occurs far from the structural perturbation, local measures show a limited efficiency. This is a first step for the description of the connection between the molecular structure and conductance in molecular switches.

Received 1st December 2015,
Accepted 20th January 2016

DOI: 10.1039/c5cp07411h

www.rsc.org/pccp

Introduction

Nowadays, research in molecular electronics focuses on the inclusion of small active molecules into electronic circuits. In those systems, the molecular switching elements carry out electronic functions such as diodes, transistors and switches. A spectacular example is a molecular four-level conductance switch based on single proton transfer in a porphyrin derivative.[1] In molecular electronics, the investigation of molecular switching elements with a panel of functions provides future prospects for miniaturization in the field of nanotechnology. Molecular switches are regarded as the most basic component in molecular electronic devices that can reverse from an active/on state to a passive/off state. The switch between two or more states with distinct properties is triggered by external stimuli such as light, pH or voltage.[2] As opposed to normal switches, molecular switches are extremely tiny and their application in nanotechnology, biomedicine and computer chip design opens up a new horizon.

In recent years, there has been a considerable growth in research on expanded porphyrins.[3,4] Owing to their tunable photophysical and chemical properties with external stimuli, expanded porphyrins represent a very promising platform to develop molecular switches for molecular electronic devices.[5–7] The most fascinating property of expanded porphyrins is their capacity to switch between several distinct π-conjugation topologies with different absorption and emission spectra.[8] Interestingly, recent experimental studies[9] proved that the photophysical properties of porphyrins are closely related to their molecular conformation and macrocyclic aromaticity. Such a change of topology is coupled to a Hückel–Möbius aromaticity

[a] *Eenheid Algemene Chemie (ALGC), Vrije Universiteit Brussel (VUB), Pleinlaan 2, 1050 Brussels, Belgium*
[b] *Sorbonne Universités, UPMC Univ. Paris 06, UMR7616, Laboratoire de Chimie Théorique, F-75005, Paris, France. E-mail: contrera@lct.jussieu.fr*
[c] *Department of Physical Chemistry, University of Vigo, Lagoas-Marcosende s/n, 36310 Vigo, Spain*
[d] *CNRS, UMR 7616, Laboratoire de Chimie Thérique, F-75005, Paris, France*
† Electronic supplementary information (ESI) available. See DOI: 10.1039/c5cp07411h

switch in a single molecule. Moreover, the topology switching is achieved by variation of one internal dihedral angle and, if properly controlled, can provide access to molecular switches with unique optical and magnetic properties. However, despite their potential, the design of molecular switches based on expanded porphyrins has only been scarcely investigated.[6,10,11]

Octaphyrins, which are composed of eight pyrrole rings, hold a unique place among expanded porphyrins: their figure-eight conformation displays two-metal coordination and intrinsic chirality.[8,12,13] The aim of this paper is to obtain qualitative insight into the conductance of octaphyrins as a function of their molecular conformation using the concept of bond metallicity. More specifically, understanding the locality of conductance changes with respect to the variation of the internal dihedral angles is crucial for the design of improved molecular switches.

However, the most common measures of metallicity are not local. For example, a metallic bond will be associated with a large local density of states at the Fermi level. Similarly, it is known that the ''nearsightedness'' of the off-diagonal terms in the first-order density matrix increases as the band gap increases.[14–17] The problem with these forms is that they require non-local information and this means that the connexion with real space (molecular structure, bonds and dihedral angles) is lost. Several local indicators have been recently proposed in the literature.[18–20] This contribution aims at understanding and establishing the structure–property relationship between molecular conformation and molecular conductance in octaphyrins using the concept of bond metallicity, which so far has only been applied to solids.

Our paper will proceed as follows. We will start by introducing the various indexes related to bond metallicity developed in the literature. Then, we will perform a proof of principle. We will test the implementation of these indexes on different molecular systems in order to assess their performance and limitations, their ability to reveal conductance and the subtleties of a topological switch. Finally, these indices will be applied to Hückel and Möbius conformations of octaphyrins in order to understand the locality of the conductivity changes upon dihedral rotation and when this assumption stays valid. This insight might help in the design of improved topological switches.

Methodology

There have been several approaches to tackle conductivity from local measures. The most common approach is to resort to density-related values at the bond critical point as originated from Atoms In Molecules (AIM).[21–26]

Within AIM, one commonly characterizes chemical bonds using the properties of the electron density at the bond critical point (bcp). In an ordinary molecule, the electron density has maxima (cusps) at the nuclei and decays exponentially as the electron density moves away from the nuclei. The resulting topology looks like an assemblage of mountains, each of which is identified as an atom. The mountain pass would then represent the bond, and its lowest point identifies the presence of such a connection, which is where their name (bond critical point, bcp) stems from.

A somewhat different approach, which requires comparing different critical points, was proposed by Mori-Sanchez *et al.*[27] Although this approach allows one to distinguish covalent, ionic, and metallic bonds, it does not provide a truly local measure of metallicity, as related to a given bond. Thus, we will concentrate on the measures uniquely related to bcps.

In 2009, Jenkins proposed a bond metallicity index based on the electron density and its Laplacian at the bond critical point $\rho(r_{\mathrm{bcp}})$ and, $\nabla^2\rho(r_{\mathrm{bcp}})$, respectively. The sign of the Laplacian determines the interaction type, distinguishing from closed shell, such as ionic or metallic (positive Laplacian) and shared or covalent interactions (negative Laplacian). Thus when looking at these measures and metallicity, one concentrates only on bcps with positive Laplacian values.[28]

$$\xi_{\mathrm{j}}(r_{\mathrm{bcp}}) = \frac{\rho(r_{\mathrm{bcp}})}{\nabla^2\rho(r_{\mathrm{bcp}})} \tag{1}$$

However ξ_{j} is neither dimensionless nor defined for singular Laplacian. Thus a revised version overcoming these flaws was proposed:[19]

$$\xi_{\mathrm{m}}(r_{\mathrm{bcp}}) = \frac{36(3\pi^2)^{2/3}\rho(r_{\mathrm{bcp}})^{2/3}\xi_{\mathrm{j}}(r_{\mathrm{bcp}})}{5} \tag{2}$$

Based on the value of ξ_{m} and ξ_{j}, at a bcp with positive Laplacian (*i.e.* at non covalent interactions), metallic bonds can be distinguished from non-metallic bonds. For instance, metallic bonds are characterized by ξ_{m} superior to 25 whereas ξ_{m} values between 5 and 25 indicate a partial metallic character. Weak metallic bonds are identified by ξ_{m} values between 1 and 5. When ξ_{m} is inferior to 1, the bonds present a non-metallic character.

Still focusing on the bcps, local metallicity measures have also been introduced in terms of kinetic energy densities and delocalization measures. In our work, we will consider three types: the electron localization function or ELF, kinetic energy density based measures (where ELF could be included according to Savin's interpretation[29]) and the local covariance.

According to the formulation of Becke and Edgecombe,[30] ELF measures the probability of finding an electron in the vicinity of another electron with the same spin:

$$\mathrm{ELF} = \frac{1}{1+\left(\frac{D}{D_{\mathrm{h}}}\right)^2} = \frac{1}{1+\chi^2} \tag{3}$$

In Savin's interpretation,[29] D corresponds to the difference between the true kinetic energy density and Weizsäcker's kinetic energy density (*i.e.* for a bosonic system), whereas D_{h} denotes the Thomas–Fermi kinetic energy density. The variable χ provides a measure of the effect of the Pauli principle in the kinetic energy density.

In highly localized regions such as covalent bonds or nuclei, ELF approaches 1. ELF is equal to 0.5 in the uniform electron gas (*i.e.* in a perfectly delocalized system). ELF can be used to understand electron delocalization when analysed in between

ELF basins[31] (*e.g.* around intermolecular bcps). In these cases, high ELF values identify delocalization in between localized regions.[32] This explains why ξ_m is positively correlated with the electron localization function at positive Laplacian bcps.[33]

In addition, localized orbitals can also be a useful tool for metallicity measures.[34] The localized orbital locator (LOL or t_{sb}) reflects the localization of orbitals in electronic systems compared with the uniform electron gas and presents values superior to 1 for highly localized systems such as covalently bound valence electrons.[35,36]

$$t_{sb}(r_{bcp}) = \frac{2\tau_{TF}(r_{bcp})}{3\tau(r_{bcp})\rho(r_{bcp})} \quad (4)$$

where τ refers to the kinetic energy density and τ_{TF} to the kinetic energy density of the homogeneous electron gas (Thomas–Fermi). Values of $t_{sb} < 1$ imply that the region is depleted in electrons with respect to the uniform gas.[37] Therefore, as the bond metallicity and t_{sb} are positively correlated to the electron density at the bond critical point, they will decrease with increasing delocalization.

In addition, the delocalization indicator, present in the definition of ELF, can also be rewritten in terms of the electron density and the local temperature. The local temperature corresponds to the ratio of kinetic energy density over the electron density and is thus inversely proportional to the bond metallicity.[38]

$$\chi(r_{bcp}) = \frac{\tau(R) - \tau_w(R)}{\tau_{TF}} = \frac{\frac{3}{2}\rho(R)\theta(R) - \tau_w(R)}{\tau_{TF}} \quad (5)$$

As demonstrated by S. Jenkins and co-workers, it is possible to apply the gradient expansion approximation to explore the link between the different metallicity measures. In the gradient expansion approximation, the kinetic energy density is expanded as the sum of the Thomas–Fermi[39,40] and Weizsäcker's kinetic energy densities[40] and the Laplacian.[41]

$$\tau = \tau_{TF} + \frac{1}{9}\tau_W - \frac{1}{6}\nabla^2\rho \quad (6)$$

$$\tau_{TF} = \frac{3(3\pi^2)^{2/3}\rho(r_{bcp})^{5/3}}{10} \quad (7)$$

$$\tau_W = \frac{\nabla\rho\nabla\rho}{8\rho} \quad (8)$$

As a result, we can approximate the localized orbital locator t_{sb} in terms of the bond metallicity index:

$$t_{sb} \approx \frac{\xi_m(r_{bcp})}{1 + 4\xi_m(r_{bcp})} \quad (9)$$

Since the electron delocalization function in ELF can be expressed in terms of the local temperature, it is also possible to establish a link between ELF and the bond metallicity. At bond critical points, we observe that the electron delocalization is related to the inverse of the bond metallicity.

$$\chi(r_{bcp}) \approx 1 + \frac{4}{\xi_m(r_{bcp})} \quad (10)$$

One has to keep in mind that the gradient expansion approximation is only valid for regions with a low electron localization ($t_{sb} < 1$) and does not provide reliable results for highly localized systems ($t_{sb} \gg 1$). Thus, as long as we stay within weak interactions (positive Laplacian, low density), the approximation should hold.

Computational details

All calculations were performed with the Gaussian suite of programs.[42,43] The geometries of the different conformations of unsubstituted [36]octaphyrins were optimized and characterized by harmonic frequency calculations with the M06 functional and the 6-31G(d,p) basis set. Single point calculations with the extended 6-311+G(d,p) basis set were also performed in order to compute more accurate electronic energies. One-dimensional relaxed scans were computed at the M06/6-31G(d,p) level of theory in order to locate the transition states and interconversion pathways for the most stable conformations. Metallicity measures were implemented in Topmod.[44] An in-house code was used for the search of critical points.

Results

The optical and aromatic properties of expanded porphyrins are highly dependent on their π-conjugation topology.[12,45] Since aromaticity is associated with electron delocalization,[46] our ultimate aim is to check how the conductivity changes upon the topology switching. However, since the approaches introduced above have been mainly applied to solids,[18–20,33] the first section is devoted to a proof of principle of the applicability of the local metallicity indexes to small molecules. Based on the results from the first section, we then analyse how these indices change as a function of the topology in octaphyrins and check the locality of the changes introduced by molecular conformation.

Proof of principle

This proof of principle addresses three fundamental questions whose answers determine the applicability of the local concept of metallicity to octaphyrins: (i) check which indices correctly reflect local metallicity (and their mutual coherency), specially upon molecular twisting (ii) check whether they reflect conductivity changes in a qualitative manner and (iii) evidence the locality of conductivity in small molecular switches and thus, the applicability of the indexes to octaphyrins.

(i) Comparison of indexes. To check the performance of local metallicity indexes in molecules, we have chosen a set of small metallorganic complexes. Our first test set is a series of complexes (Fig. 1) consisting of hexafluorophenyl and a small molecule (LiH, FH, NH_3, H_2O, HCN, CNH) because of the wide range of interactions as well as their simplicity.[47] Optimizations were done with the CAM-B3LYP/6-31G(d,p) functional to avoid delocalization errors in the complexes. We have tested three types of indexes introduced in the Methodology section as well as the performance of their approximate gradient expansion expressions.

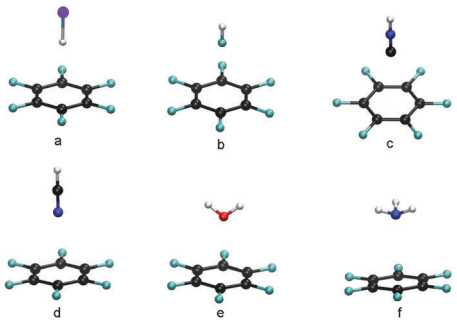

Fig. 1 Hexafluorophenyl complexes. (a) LiH, (b) FH, (c) CNH, (d) HCN, (e) H_2O, (f) NH_3.

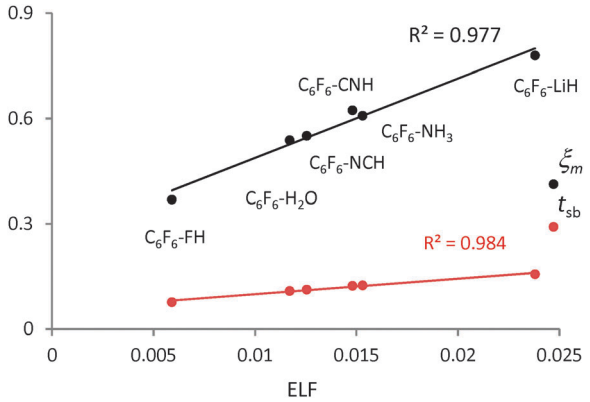

Fig. 2 Correlation between bond metallicity and the localized orbital locator with ELF values for systems in Fig. 1.

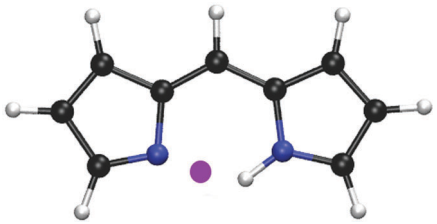

Fig. 3 Bond critical point representing the hydrogen bonding in the dipyrromethene molecule.

The aim of this test is to check the delocalization within the system and the ability of the above indexes to reflect the delocalization through space, capabilities that are necessary to analyse cyclic systems.

According to Table 1, the LiH- and the FH-hexafluorophenyl complexes present the highest and the lowest ξ_m and ELF values, respectively. According to their ξ_m values, none of the system presents a metallic bond but those with higher ξ_m values tend to display non-covalent bonds which would fall in the very weak metallic character range. The trend can be understood in terms of the electronegativity of the atom and the delocalized nature of the electrons facing the ring. In the case of LiH, the H atom faces the ring, whereas it is the atom X in the X(Y)H complexes the one that is closer to the ring in the rest of the cases. H atom, being very diffuse, comes first in the series. Then the rest of the complexes are ordered in terms of electronegativity: C, N, O and F. It is interesting to note that NH_3 and CNH lay very close in all measures.

As shown in Fig. 2, the measures of metallicity based on the kinetic energy t_{sb} and the bond metallicity ξ_m present an excellent correlation with ELF values at the bond critical point. According to Table 1 and Fig. 2, the orbital localization and the bond metallicity increase with the ELF values from the C_6F_6–FH to the C_6F_6–LiH complex. Approximating this relationship by a straight line, correlations coefficients close to 1 are obtained, much simpler than the relationship expected from the eqn (8) and (9).

Table S1 (ESI†) collects the metallicity measures computed with the gradient expansion approximation (GEA). In general, the expansion provides results in good agreement with the original data (Table 1). Owing to the excellent correlation between ELF and the measures of metallicity within the GEA framework ($R^2(\xi_m) = 0.967$ and $R^2(\chi) = 0.972$), we will employ the GEA approximation of ξ_m and χ to evaluate the metallicity in the next systems.

Table 1 Metallicity measures of CAM-B3LYP/6-31G(d,p) optimized structures at the bond critical points between the small molecule and the aromatic ring (systems in Fig. 1)

	Name	ξ_m	ELF	t_{sb}
a	C_6F_6–LiH	0.779	0.024	0.156
c	C_6F_6–CNH	0.608	0.015	0.125
f	C_6F_6–NH_3	0.623	0.015	0.123
d	C_6F_6–NCH	0.551	0.012	0.113
e	C_6F_6–H_2O	0.538	0.012	0.109
b	C_6F_6–FH	0.369	0.006	0.077

Since we want to apply these indexes to analyse the changes of conductivity along the rotation of C–C bonds in octaphyrins, it is important to first check whether they are able to go beyond the identification of changes in delocalization among different compounds and characterize relative delocalization upon rotation of a given molecule. We have analysed the twisting in dipyrromethene since it shows a similar structure to octaphyrins. Dipyrromethene presents a bond critical point between its imino and amino group (Fig. 3) until the central torsional angle reaches 50°, value at which the hydrogen bond vanishes. This is an intrinsic drawback of these local quantities: they cannot be measured beyond bcp coalescence.[48]

The measures of metallicity of the dipyrromethene indicate that the metallicity decreases upon rotation. This can be understood as a reduction of π-conjugation, due to an elongation of the hydrogen bond (Table 2). Towards the end of the rotation, there is an important change in slope of all the metallicity indexes (Fig. 4). This is due to the fact that the hydrogen bond bcp is on the verge of disappearing.

(ii) Delocalization and conductivity. Once the ability of these indexes to identify delocalization has been settled, the question of whether this can be related to conductivity remains open. Some of the present authors, have recently investigated the electronic properties of *p*-xylylene (PX1 and PX2) and *p*-phenylene (PP) chains at different finite bias voltage (Fig. 5).[49] Due to the

Table 2 Measures of metallicity for dipyrromethene with different dihedral angles

Dihedral angle	ELF	ξ_m	t_{sb}	d^a
0	0.122	2.257	0.362	2.017
10	0.119	2.215	0.356	2.031
20	0.108	2.082	0.342	2.069
30	0.090	1.854	0.317	2.139
40	0.067	1.519	0.275	2.256

[a] d stands for the hydrogen bond distance in Å.

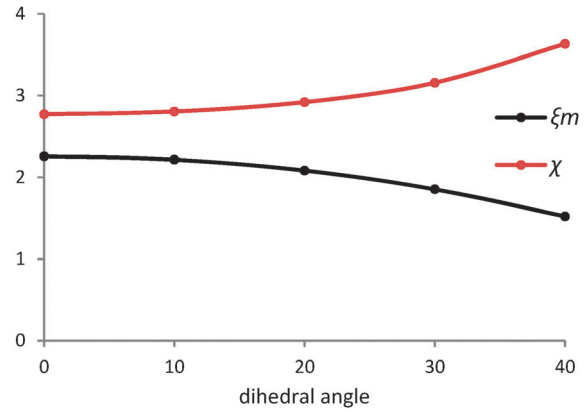

Fig. 4 Evolution of several indices of metallicity with the dihedral angle of dipyrromethene.

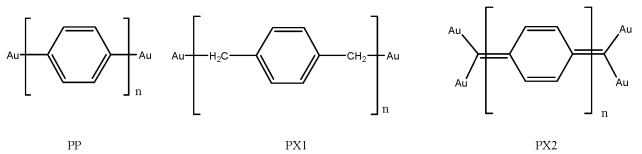

Fig. 5 Investigated p-phenylene (PP) and p-xylylene (PX1 and PX2) units.

covalent bond between the gold atom and the carbon chain in PX, xylylene presents higher conductivity than PP, where the bond to the benzene unit is direct. Moreover, the response to an applied external voltage is different for these three structures. For instance, the applied external voltage induces a higher delocalization in PX2 as the voltage and the number of ring increases. Instead, the external voltage destroys the delocalization in PX1 and PP, which leads to a reduction of the delocalization as the number of rings and the voltage increase.

We have compared the metallicity indexes with the intensity and voltage results from ref. 49. All the measures of metallicity were computed at the junction between the gold atom and the organic part of the molecule. The bond metallicity, the delocalization indicator computed with the gradient expansion approximation, the voltage and the current intensity are collected in Table 3 for p-phenylene with one and two subunits. Owing to the presence of Au atoms, the bond between Au and the organic moiety lies in the intermediary metallic range (ξ_m within 5–25). The metallicity of the system increases with the current intensity (Fig. 6) whereas the delocalization of electrons is inversely proportional to the current intensity (Fig. S3, ESI†). Both measures

Table 3 Induced current density, metallicity index and delocalization indicator for p-phenylene (PP) with one (n1) and two (n2) phenyl rings. Intensity in microamperes and voltage in volts

V	I(n1)	ξ_m(n1)	χ(n1)	I(n2)	ξ_m(n2)	χ(n2)
0	0.000	15.545	1.257	0.000	15.672	1.255
0.5	0.072	12.570	1.318	0.033	15.702	1.255
1.5	2.093	13.540	1.295	0.814	16.056	1.249
2.5	9.766	14.812	1.270	3.891	16.833	1.238
3.5	27.398	22.000	1.182	10.317	18.180	1.220

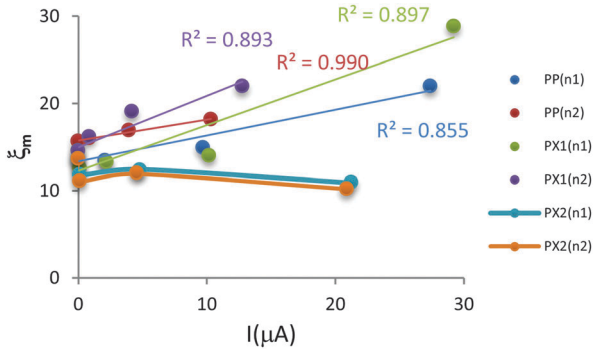

Fig. 6 Relation of the bond metallicity with the induced current for PP, PX1 and PX2.

of metallicity (ξ_m and χ) are correlated to the current intensity ($R^2 > 0.98$) and at a lower extent to the voltage ($R^2 > 0.90$) (see Fig. S4, ESI†). Moreover, the phenylene chain with two ring subunits displays higher metallicity than its homologous chain with one subunit (Fig. 6). In addition, the delocalization of the electrons decreases with the applied voltage, more rapidly in p-phenylene with one subunit, falling very rapidly at high voltage (Fig. S5b, ESI†). This reduction of the delocalization indicator is in agreement with the results from ref. 49, which showed that the delocalization was destroyed at higher voltage in PP.[49]

p-Xylylene PX1 behaves similarly with the external perturbation as PP because the bond metallicity increases with induced current and applied voltage (Fig. 6 and Fig. S6, ESI†). However, PX1 possesses higher molecular conductance, which can be related to its higher metallicity (Table 4). Although our index faces some troubles to estimate the metallicity measures at V = 0.5 V, it provides a qualitative picture of the evolution of the system which is in agreement with the observations of Ramos-Berdullas *et al.*[49]

PX1 follows a similar trend as PP with the voltage. The metallicity index is inversely related to the voltage and the number of subunits (Fig. 6 and Fig. S6, ESI†). However, the localization of

Table 4 Induced current density, metallicity index and delocalization indicator for p-xylylene (PX1) with one (n1) and two (n2) phenyl rings. Intensity in microampers and voltage in volts

V	I(n1)	ξ_m(n1)	χ(n1)	I(n2)	ξ_m(n2)	χ(n2)
0	0.000	14.451	1.277	0.000	14.594	1.274
0.5	0.074	12.530	1.319	0.030	13.700	1.292
1.5	2.190	13.342	1.299	0.921	16.123	1.248
2.5	10.198	14.014	1.285	4.186	18.989	1.231
3.5	29.202	28.823	1.139	12.758	21.941	1.182

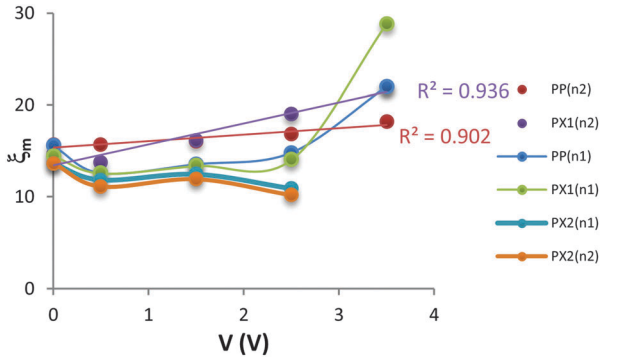

Fig. 7 Relation of the bond metallicity with the applied voltage for PP, PX1 and PX2.

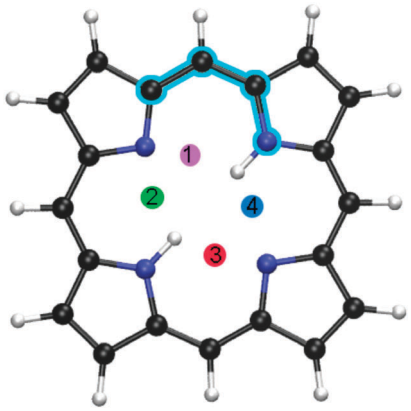

Fig. 8 Porphyrin with the investigated bond critical points coloured and numbered according to their position.

electrons is more pronounced in PX1 than in PP (Fig. 7) because the gold atoms are covalently bound to methyl groups, which seem to be more affected by the external voltage. Nevertheless, both PP and PX1 behave as bulk semiconductors.

Unlike PP and PX1, the bond metallicity index of PX2 decreases with increasing applied voltage (Fig. S7, ESI†) while the induced current still increases with the voltage (Table 5). However, PX2-n2 presents lower current intensity than PX2-n1, coupled in general to higher metallicity values (Fig. 6). In comparison with PP and PX1, PX2 presents a lower bond metallicity index at the junction between gold and the sp^2 carbon atom because the electrons are more delocalized in the whole structure. The evaluation of the bond metallicity is more problematic for the PX2-n2 structure at 0.5 V because there is a drop in bond metallicity and an increase in electron delocalization (Fig. 7 and Fig. S7, ESI†). Nevertheless, the bond metallicity still provides the correct qualitative picture because it is able to grasp the different behaviour of PX2 with respect to PP and PX1.

In contrast to PX1 and PP, the delocalization index χ generally increases with the voltage and the induced current intensity in PX2 (Fig. 7 and Fig. S7, ESI†). This opposite behaviour of the delocalization of the electrons indicates that higher voltage enhances the electrons delocalization in PX2. Moreover, the inclusion of the additional subunits in PX2 also promotes the electron delocalization in the whole molecule. Ramos-Berdullas *et al.* reported that the molecular response of PX2 to the applied voltage was not similar to that of a bulk semi-conductor.[49]

Therefore, we can say that the bond metallicity indexes provide a qualitative picture of the molecular conductance and the electronic properties of molecular semi-conductors. However, further analysis is needed in order to predict the response of a molecule belongs in the presence of metallic junctions, *e.g.* whether delocalization increases or decreases with voltage.

(iii) Is delocalization local in octaphyrins? Finally, we have assessed whether the evolution of the bond metallicity is local in macromolecular systems such as porphyrins. This last part of the proof of principle aims at exploring the local character of the metallicity measures on a Hückel–Möbius transition in regular porphyrin. According to the value of the dihedral angle d, porphyrin presents a Hückel ($d < 90°$) or a Möbius topology ($d > 90°$). The Hückel topology contains formal *cis* bonds in the smallest macrocyclic pathway, whereas in the Möbius conformation there is one *trans* bond. The AIM topological analysis reveals that four bond critical points with positive Laplacian are present, which correspond to the four hydrogen bonds (see Fig. 8).

In Fig. 8, the bond critical point 1 (in purple) is always used to refer to the bond critical point that is the closest to the perturbation. If conductivity remains local in these switches, we expect the variation of the measure of the metallicity to be maximal at the perturbation (bcp1) and to become less important with increasing distance from the twist.

We observe that ELF and ξ_m evolve similarly with the dihedral angle (Fig. 9 and Fig. S8, ESI†). The bond metallicity decreases at all bond critical points except for the bond critical point 2 where the reverse situation is observed. In order to compensate the loss of hydrogen bonds, the hydrogen bond above the bond critical point 2 is strengthened, resulting in increased bond metallicity at this point. The biggest variations in metallicity are observed in bcp2 and bcp4, which are the closest ones to the rotating dihedral angle, whereas the metallicity in bcp3 (which is the furthest bcp) is less affected. It is interesting to note, that the metallicity of bcp3 appears to mimic that of bcp1 before it disappears.

Table 5 Induced current density, metallicity index and delocalization indicator for *p*-xylylene (PX2) with one (n1) and two (n2) phenyl rings. Intensity in microampers and voltage in volts. Results at V = 3.5 V have not been included due to problems with the critical point search

V	I(n1)	ξ_m(n1)	χ(n1)	I(n2)	ξ_m(n2)	χ(n2)
0	0.000	13.617	1.294	0.000	13.646	1.293
0.5	0.162	11.829	1.338	0.172	11.112	1.359
1.5	4.761	12.450	1.321	4.492	11.917	1.335
2.5	21.196	10.888	1.368	20.948	10.168	1.393

Octaphyrins

In order to gain a qualitative insight into the evolution of the bond metallicity in octaphyrins, two interconversions of

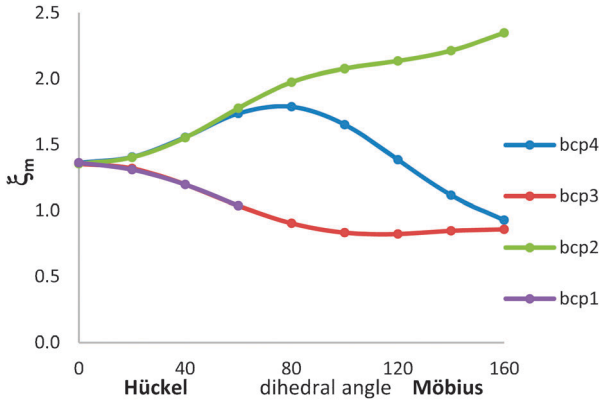

Fig. 9 Evolution of the bond metallicity as function of the amplitude of the dihedral angle in porphyrin. Colours follow the pattern in Fig. 8.

octaphyrins were investigated. Since the interconversion between different conformers relies on the variation of one or two dihedral angle(s),[6] we expect the variation of the bond metallicity to be local, and thus our indices to be applicable. Moreover, based on the study of *p*-phenylene and *p*-xylylene, we have also seen that the bond metallicity and the delocalization indicator are related to the current intensity. Thus, since Möbius and Hückel expanded porphyrins exhibit distinct aromatic and optical properties, the molecular conductance could also be expected to be topology-dependent.

Firstly, we investigated a two-step interconversion between two Möbius structures (**M1**, **M2**) involving an intermediary Hückel topology **H1** (Fig. 10 and 11). The rotating dihedral angle is denoted in light blue. In contrast to the previous interconversion, the rotation of the *cis* dihedral angle in **M1** induces an additional rotation of the neighboring pyrrole ring, giving rise to an extra hydrogen bond in structures **H1** and **M2**.

The bond metallicity is highly correlated to the ELF value for these conformers ($R^2 > 0.99$, Fig. S10, ESI†). Following from our analysis on the regular porphyrin, we have only investigated half of the critical points in the octaphyrin macrocycle, focusing on the side of the rotating dihedral angle. We use the same nomenclature as above, with the bond critical point next to the perturbation denoted as 1 and the index keeps increasing in a clock-wise manner. Thus, 2 and 8 are the closer bcps to the perturbation and so on.

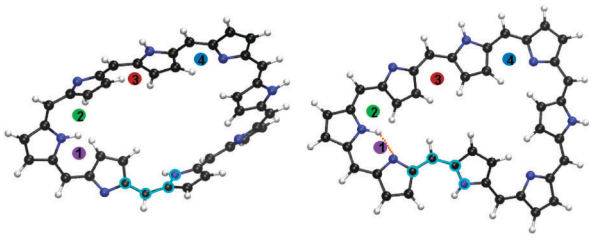

Fig. 10 Investigated bond critical points in the molecular switch, where the rotating dihedral angle is highlighted in light blue. The bcps are numbered like in the text and colored like in the graphs. The new hydrogen bond in the H1 structure is highlighted with a red dotted line.

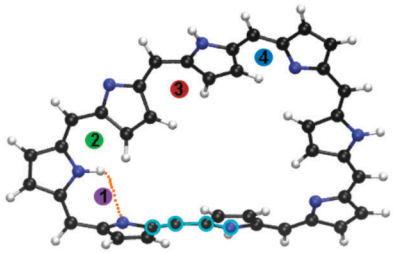

Fig. 11 Investigated bond critical points in the molecular switch, where the varying dihedral angle is highlighted in light blue. The bcps are numbered like in the text and colored like in the graphs. The new hydrogen bond is highlighted with a red dotted line.

The changes induced by the topological switch are extremely local in nature. The variation of the bond metallicity at bcps 2, 3, 4 are negligible with respect to that of bcp1 (Fig. 12 and Fig. S11, ESI†). The bond metallicity of bcp1 increases dramatically when the dihedral angle reaches 60° for **H1** and **M2** (Table S2, ESI†). This increase is due to the formation of a hydrogen bond indicated in red in Fig. 10 and 11. For the same non-covalent interaction framework (**H1** and **M2**), Hückel leads to a better conductance, but the biggest structure-conductance change is expected as the **M1**–**H1** conformational change is induced. This is specially so if we take into account that bcp1 was initially the one that was related to the lowest metallicity, and hence, it could be thought of as the conductance limiting step.

As a second study case, we investigated a one-step Hückel–Möbius interconversion that displays a smooth potential energy surface (Fig. S12, ESI†). This Hückel–Möbius transition corresponds to the untwisting of the twisted-Hückel conformer H2 (Fig. 13) that results in the Möbius conformer **M3** (Fig. 14). The bond critical point above the changing dihedral angle is denoted again as bcp1 and the following bcps are named clockwise from this point on, so that the bcps close to the perturbation are again bcp2 and bcp8. The interesting thing about this transformation is that a π–π staking interaction appears at the half-twist (**H2**), which is denoted as bcp9. The bcps close to this π–π interaction are bcp6 and bcp9 in our graphs (Fig. 13).

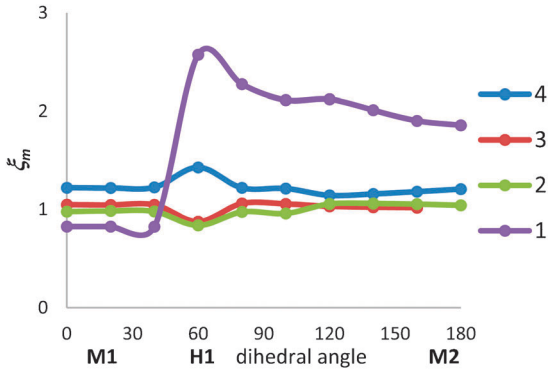

Fig. 12 Evolution of the bond metallicity with the amplitude of the dihedral angle (molecules **M1**, **H1**, **M2**).

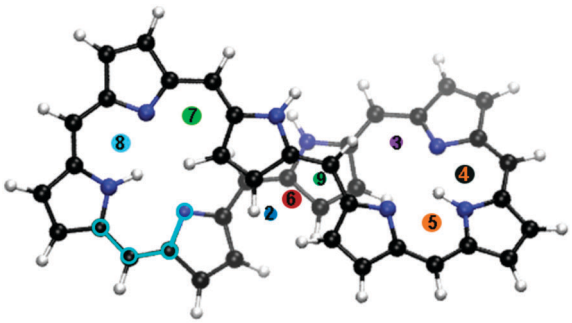

Fig. 13 Hückel topology **H2** with the bond critical points colored according to their position the varying dihedral angle is highlighted in light blue.

Although the electron density topological analysis carried out with our modified version of TOPMOD reveals 11 non-covalent bcps at the global minimum of the PES (**H2**, $d = 0^\circ$), we only evaluated measures of metallicity at the most important bcps (8 in total). In fact, according to the evolution of the Laplacian during the interconversion, several non-covalent interactions gradually disappear as the amplitude of the dihedral angle increases. Since bcp1 was soon undetectable, its measures of metallicity were not used in the analysis of the macrocycle.

The bond metallicity ξ_m changes are depicted in Fig. 15. They remain highly correlated to ELF values during the whole interconversion ($R^2 > 0.93$, Table S3 and Fig. S13, ESI†). The bond critical points lying in the vicinity of the perturbation (bcp8, bcp2) are more sensitive to the variation of the dihedral angle, highlighting the local nature of the metallicity in this system. However, since the Hückel–Möbius transition involves the creation of a π–π staking interaction, the corresponding bcp (bcp9) and its neighbor (bcp6) also present a non-negligible variation. In fact, owing to the loss of a π–π stacking interaction, the bond metallicity of bcp5 and bcp9 decreases for larger amplitudes of the dihedral angle.

Delocalization at the bcps close to the twist (bcp2, bcp6 and bcp8) increases when going from the twisted-Hückel **H2** to the Möbius topology **M3**. This behavior differs slightly from one index to another. In comparison to the bond metallicity, the delocalization index seems to be less position dependent. All in all, although the bcp closest to the perturbation still presents the highest variation in the measures of metallicity, delocalization is not fully local since the important changes also occur associated to the folding.

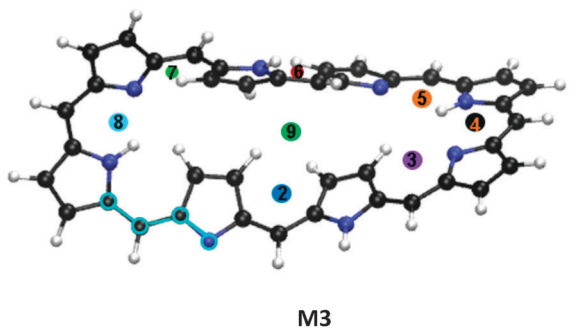

Fig. 14 Möbius topology **M3** with the bond critical points colored according to their position and the rotating dihedral angle is highlighted in light blue.

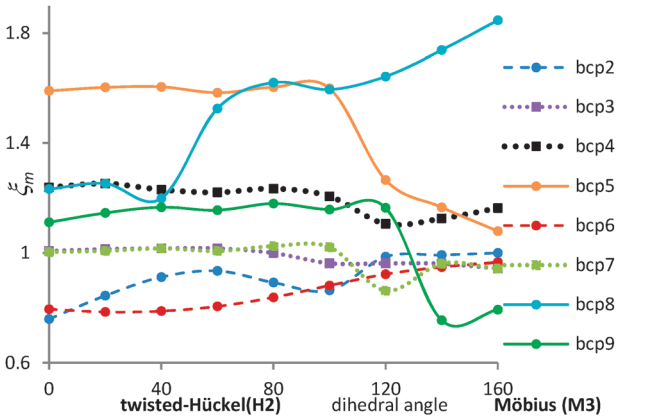

Fig. 15 Evolution of the bond metallicity index at several critical points of the molecule with the amplitude of the dihedral angle (rotation from **H2** to **M3**).

Thus, we have seen that local measures of metallicity are able to cast the changes in delocalization upon conformational switch in octaphyrins. In those cases where the conformation remains open (so that there is no net change of interactions associated with the twist), the changes remain rather local, which can be used in the qualitative prediction of delocalization and conductivity in porphyrins and expanded porphyrins. In those cases where there is a fold, the change in interactions introduces a non local behavior which has to be taken into account.

Conclusions

We have reviewed several local indexes of metallicity based on the analysis of electron density, ELF and the kinetic energy density at the bond critical point. Since these quantities have usually been applied to solid state, we have first analysed its applicability to molecules. Firstly, we have seen that these measures are mutually coherent and that they can be used in very small molecular switches. Next, the relationship between the bond metallicity index and conductivity was probed. We have seen that the delocalization indicator is able to provide a qualitative picture of the electronic properties of *p*-phenylene and *p*-xylylene chains that is in agreement with the molecular conductance of both systems. Finally, we checked a larger system to test the applicability of local indexes to describe changes in a switch. We found that delocalization in model small switches is a local quantity because their variation is less pronounced far from the perturbation.

Based on these results, we have tested two topological switches based on the [36]octaphyrin. Our results demonstrated that the bond metallicity and delocalization index provide a qualitative description of the electron delocalization in octaphyrins, which are in agreement with ELF topological analysis. According to the

measures of bond metallicity, we observed that the variation of the electron delocalization was local when the topological change was restricted to one part of the molecule and semi-local for global topological changes (*e.g.* folding). In the local cases, our approach enables to identify which conformational switch would be more efficient from an electronic device perspective. As our indices were able to grasp the difference between those two interconversions, they could also be used to perform a qualitative analysis in octaphyrins. These studies are expected to be applicable to other macrocycles and will be the object of future studies.

Acknowledgements

M. A. thanks the Fund for Scientific Research-Flanders FWO for a postdoctoral fellowship (12F4416N) and the Free University of Brussels (VUB) for financial support. F. D. P. wishes to acknowledge the VUB for a Strategic Research Program.

References

1 M. Jurow, A. Schuckman, J. Batteas and C. Drain, *Coord. Chem. Rev.*, 2010, **254**, 2297–2310.
2 (*a*) B. L. Feringa and W. R. Brwone, *Molecular Switches*, Wiley-VCH, Weinheim, Germany, 2011; (*b*) J. Andréasson and U. Pischel, *Chem. Soc. Rev.*, 2010, **39**, 174–188; (*c*) B. Gui, X. Meng, Y. Chen, J. Tian, G. Liu, C. Shen, M. Zeller, D. Yuan and C. Wang, *Chem. Mater.*, 2015, **27**, 6426–6431; (*d*) T. Woller, J. Contreras-García, P. Geerlings, F. De Proft and M. Alonso, *Phys. Chem. Chem. Phys.*, 2016, DOI: 10.1039/C5CP07413D.
3 M. Stępień, B. Szyszko and L. Latos-Grażyński, *J. Am. Chem. Soc.*, 2010, **132**, 3140–3152.
4 M. Stępień, N. Sprutta and L. Latos-Grażyński, *Angew. Chem., Int. Ed.*, 2011, **50**, 4288–4340.
5 S. Saito and A. Osuka, *Angew. Chem., Int. Ed.*, 2011, **50**, 4342–4373.
6 M. Alonso, P. Geerlings and F. De Proft, *Chem. – Eur. J.*, 2013, **19**, 1617–1628.
7 M. Torrent-Sucarrat, J. M. Anglada and J. M. Luis, *J. Chem. Phys.*, 2012, **137**, 184306.
8 G. Karthik, J. Min Lim, A. Srinivasan, C. H. Suresh, D. Kim and T. K. Chandrashekar, *Chem. – Eur. J.*, 2013, **19**, 17011–17020.
9 D. Hrsak, M. A. Pertejo, Al. M. Lamshabi, A. Muranaka and A. Ceulemans, *Chem. Phys. Lett.*, 2013, **586**, 148–152.
10 M. Alonso, P. Geerlings and F. De Proft, *Chem. – Eur. J.*, 2012, **18**, 10916–10928.
11 M. Alonso, P. Geerlings and F. De Proft, *Phys. Chem. Chem. Phys.*, 2014, **16**, 14396–14407.
12 J. M. Lim, J.-Y. Shin, Y. Tanaka, S. Saito, A. Osuka and D. Kim, *J. Am. Chem. Soc.*, 2010, **132**, 3105–3114.
13 J. Y. Shin, K. S. Kim, M. C. Yoon, J. M. Lim, Z. S. Yoon, A. Osuka and D. Kim, *Chem. Soc. Rev.*, 2010, **39**, 2751–2767.
14 W. Kohn, *Phys. Rev. Lett.*, 1996, **76**, 3168–3171.
15 T. Marino, M. C. Michelini, N. Russo, E. Sicilia and M. Toscano, *Theor. Chem. Acc.*, 2012, 131–141.
16 X. P. Li, W. Nunes and D. Vanderbilt, *Phys. Rev. B: Condens. Matter Mater. Phys.*, 1993, **47**, 10891–10894.
17 R. Baer and M. Head-Gordon, *Phys. Rev. Lett.*, 1997, **79**, 3962–3965.
18 S. Jenkins, *J. Phys.: Condens. Matter*, 2002, **14**, 10251–10263.
19 P. W. Ayers and S. Jenkins, *Comput. Theor. Chem.*, 2014, **1053**, 112–122.
20 N. Seriani, *J. Phys.: Condens. Matter*, 2010, **22**, 255502.
21 R. F. W. Bader, *Atoms in Molecules: A Quantum Theory*, Clarendon, Oxford, 1990.
22 R. F. W. Bader and T. T. Nguyendang, *Adv. Quantum Chem.*, 1981, **14**, 63–124.
23 P. L. A. Popelier, *Atoms in Molecules: An Introduction*, Pearson, Harlow, 2000.
24 C. F. Matta and R. F. W. Bader, *J. Phys. Chem. A*, 2006, **110**, 6365–6371.
25 R. F. W. Bader, *J. Phys. Chem. A*, 1998, **102**, 7314–7323.
26 R. F. W. Bader, Y. Tal, S. G. Anderson and T. T. Nguyen-Dang, *Isr. J. Chem.*, 1980, **19**, 8–29.
27 P. Mori-Sanchez, A. M. Pendas and V. Luana, *J. Am. Chem. Soc.*, 2002, **124**, 14721–14723.
28 S. Jentkins, *J. Phys.: Condens. Matter*, 2012, **14**, 10251–10263.
29 A. Savin, O. Jepsen, J. Flad, O. K. Andersen, H. Preuss and H. G. von Schnering, *Angew. Chem., Int. Ed.*, 1992, **31**, 187.
30 A. D. Becke and K. E. Edgecombe, *J. Chem. Phys.*, 1990, **92**, 5397–5403.
31 J. Contreras-Garcia and J. M. Recio, *Theor. Chem. Acc.*, 2011, **128**, 411.
32 B. Silvi and C. Gatti, *J. Phys. Chem. A*, 2000, **104**, 947–953.
33 S. Jenkins, S. R. Kirk, P. W. Ayers and W. F. Kuhs, *R. Soc. Chem.*, 2006, 265–272.
34 V. Tsirelson and A. Stash, *Chem. Phys. Lett.*, 2002, **351**, 142–148.
35 H. L. Schmider and A. D. Becke, *J. Chem. Phys.*, 2002, **116**, 3184–3193.
36 H. L. Schmider and A. D. Becke, *THEOCHEM*, 2000, **527**, 51–61.
37 S. Jenkins, P. W. Ayers, S. R. Kirk, P. Mori-Sánchez and A. Martín Pendás, *Chem. Phys. Lett.*, 2009, **1**, 174–177.
38 S. K. Ghosh, M. Berkowitz and R. G. Parr, *Proc. Natl. Acad. Sci. U. S. A.*, 1984, **81**, 8028–8031.
39 L. H. Thomas, *Proc. Cambridge Philos. Soc.*, 1927, **23**, 542–548.
40 E. Fermi, *Z. Phys.*, 1928, **48**, 73–79.
41 J. M. Tao, G. Vignale and I. V. Tokatly, *Phys. Rev. Lett.*, 2008, **100**, 206405.
42 M. J. Frisch, G. W. Trucks, H. B. Schlegel, G. E. Scuseria, M. A. Robb, J. R. Cheeseman, J. A. Montgomery, Jr., T. Vreven, K. N. Kudin, J. C. Burant, J. M. Millam, S. S. Iyengar, J. Tomasi, V. Barone, B. Mennucci, M. Cossi, G. Scalmani, N. Rega, G. A. Petersson, H. Nakatsuji, M. Hada, M. Ehara, K. Toyota, R. Fukuda, J. Hasegawa, M. Ishida, T. Nakajima, Y. Honda, O. Kitao, H. Nakai, M. Klene, X. Li, J. E. Knox, H. P. Hratchian, J. B. Cross,

V. Bakken, C. Adamo, J. Jaramillo, R. Gomperts, R. E. Stratmann, O. Yazyev, A. J. Austin, R. Cammi, C. Pomelli, J. W. Ochterski, P. Y. Ayala, K. Morokuma, G. A. Voth, P. Salvador, J. J. Dannenberg, V. G. Zakrzewski, S. Dapprich, A. D. Daniels, M. C. Strain, O. Farkas, D. K. Malick, A. D. Rabuck, K. Raghavachari, J. B. Foresman, J. V. Ortiz, Q. Cui, A. G. Baboul, S. Clifford, J. Cioslowski, B. B. Stefanov, G. Liu, A. Liashenko, P. Piskorz, I. Komaromi, R. L. Martin, D. J. Fox, T. Keith, M. A. Al-Laham, C. Y. Peng, A. Nanayakkara, M. Challacombe, P. M. W. Gill, B. Johnson, W. Chen, M. W. Wong, C. Gonzalez and J. A. Pople, *Gaussian 03, Revision C.02*, Gaussian, Inc., Wallingford, CT, 2004.

43 M. J. Frisch, G. W. Trucks, H. B. Schlegel, G. E. Scuseria, M. A. Robb, J. R. Cheeseman, G. Scalmani, V. Barone, B. Mennucci, G. A. Petersson, H. Nakatsuji, M. Caricato, X. Li, H. P. Hratchian, A. F. Izmaylov, J. Bloino, G. Zheng, J. L. Sonnenberg, M. Hada, M. Ehara, K. Toyota, R. Fukuda, J. Hasegawa, M. Ishida, T. Nakajima, Y. Honda, O. Kitao, H. Nakai, T. Vreven, J. A. Montgomery, Jr., J. E. Peralta, F. Ogliaro, M. Bearpark, J. J. Heyd, E. Brothers, K. N. Kudin, V. N. Staroverov, R. Kobayashi, J. Normand, K. Raghavachari, A. Rendell, J. C. Burant, S. S. Iyengar, J. Tomasi, M. Cossi, N. Rega, J. M. Millam, M. Klene, J. E. Knox, J. B. Cross, V. Bakken, C. Adamo, J. Jaramillo, R. Gomperts, R. E. Stratmann, O. Yazyev, A. J. Austin, R. Cammi, C. Pomelli, J. W. Ochterski, R. L. Martin, K. Morokuma, V. G. Zakrzewski, G. A. Voth, P. Salvador, J. J. Dannenberg, S. Dapprich, A. D. Daniels, Ö. Farkas, J. B. Foresman, J. V. Ortiz, J. Cioslowski and D. J. Fox, *Gaussian 09, Revision D.01*, Gaussian, Inc., Wallingford, CT, 2009.

44 S. Noury, X. Krokidis, F. Fuster and B. Silvi, *J. Comput. Chem.*, 1999, **23**, 597–604.

45 M.-C. Yoon, S. Cho, M. Suzuki, A. Osuka and D. Kim, *J. Am. Chem. Soc.*, 2009, **131**, 7360–7367.

46 P. Schleyer, *Chem. Rev.*, 2001, **101**, 5.

47 I. Alkorta, I. Rozas, M. L. Jimeno and J. Elguero, *Struct. Chem.*, 2001, **12**, 459–464.

48 J. R. Lane, J. Contreras-Garcia, J.-P. Piquemal, B. J. Miller and H. G. Kjaergaard, *J. Chem. Theory Comput.*, 2013, **9**, 3263–3266.

49 N. Ramos-Berdullas and M. Mandado, *Chem. – Eur. J.*, 2013, **19**, 3646–3654.

